Dynamical Spin Injection Based on Heating Effect due to Ferromagnetic Resonance

Kazuto Yamanoi,[1] Yuki Yokotani,[1] and Takashi Kimura[1,2,*]

[1]*Department of Physics, Kyushu University, 744 Motooka, Fukuoka 819-0395, Japan*
[2]*Research Center for Quantum Nano-Spin Sciences, Kyushu University, 744 Motooka, Fukuoka 819-0395, Japan*

(Received 7 September 2016; revised manuscript received 18 September 2017; published 15 November 2017)

Dynamical spin injection based on the ferromagnetic resonance is an attractive and powerful method for generating and manipulating the spin current. To date, in a ferromagnet/nonmagnet bilayer system, the spin-pumping effect from the ferromagnet into the nonmagnet has been considered only as the mechanism of the dynamical spin injection. Here, we examine another method for the dynamical spin injection based on the heating effect due to the ferromagnetic resonance in a $(\mathrm{Co,Fe})\mathrm{B}/\mathrm{Pt}$ bilayer system. The (Co,Fe)B film heated by the ferromagnetic resonance produces the temperature gradient across the $(\mathrm{Co,Fe})\mathrm{B}/\mathrm{Pt}$ interface, resulting in the thermal spin injection from the (Co,Fe)B layer into the Pt film. The obtained electrical signal clearly shows the spin Hall signature and exceeds 20 $\mathrm{mV}\,\Omega^{-1}\,\mathrm{m}^{-1}$, which is relatively large compared to the values reported in similar bilayer structures driven by spin pumping. The structural dependence of the inverse spin Hall signal and its power dependence provide consistent results with the dynamical thermal-spin-injection model due to the ferromagnetic resonance.

DOI: 10.1103/PhysRevApplied.8.054031

I. INTRODUCTION

There has been a great deal of interest in spintronic devices consisting of ferromagnetic-nonmagnetic hybrid structures since the discovery of spin-dependent transports [1]. In operations of the spintronic devices, a spin current, a flow of spin angular momentum, is a key ingredient rather than the electric current in charge-based electric devices because the magnetization can be controlled and detected by the spin current. Spin current is, in general, created by applying an electric field across the ferromagnet (FM) and nonmagnet (NM) interface, resulting in an injection of the spin-polarized electrons from the FM into the NM. This method is known as electrical spin injection, which is a powerful means for generating the spin current because of its high selectivity and flexibility [2]. Moreover, by extending the electrical spin injection to a multiterminal FM-NM hybrid nanostructure, we are now able to create pure spin current, a flow of spin angular momentum without an accompanying charge current. This pure spin current enables us to observe various intriguing spin-related phenomena sensitively because of the absence of the charge current and could be employed to transport the spin information with low power consumption [3–8]. The origin of the electrical spin injection is due to the spin dependence of the electrical conductivity. Since the Seebeck coefficient in the ferromagnet also shows the spin dependence, it is possible to inject the spin current into the nonmagnet by using the temperature gradient instead of the electric field. This method is known as thermal spin injection, where the generation efficiency often shows significant enhancement in several ferromagnetic metals, depending on its band structure.

Apart from the aforementioned static spin injection, the dynamical spin injection induced by microwave irradiation is also an attractive mean for generating and manipulating the spin current because of its simple experimental scheme. To date, the mechanism of the dynamical spin injection has been attributed to the spin pumping induced by the magnetization precession of ferromagnetic resonance (FMR) [9,10] in the FM/NM bilayer structure. The magnitude of the spin current induced by the spin pumping is evaluated from the change of the linewidth of the FMR spectra. However, the linewidth of the FMR spectra is strongly affected by the crystal and geometrical inhomogeneity, namely, inhomogeneous broadening, which makes it difficult to estimate the intrinsic and extrinsic contribution of the damping constant [11,12]. In addition, recent studies pointed out the importance of the influence of the ferromagnetic proximity effect [13] and the Dzyaloshinskii-Moriya interaction [14] on the magnetization dynamics in the bilayer system. Therefore, the linewidth of the FMR is modified not only by spin pumping but also by other additional effects. This uncertainty leads to complications for the quantitative estimation of the injected spin current due to the spin pumping. Moreover, the magnitude of the ac spin current with the precession frequency is much larger than the dc spin current in the spin-pumping mechanism [15]. However, the contribution of the ac spin current has not been considered intensively because of the difficulty of the systematic analysis. Thus, the dynamical spin injection based on spin pumping still poses various problematic issues.

*t-kimu@phys.kyushu-u.ac.jp

Here, we propose another mechanism for dynamical spin injection based on the FMR-heating effect. We recently found that heat dissipation due to FMR, which is caused by the imaginary part of the magnetic susceptibility, increases the temperature of the ferromagnet [16]. This fact indicates that the FMR-heating effect in the FM/NM bilayer structure produces the temperature gradient across the FM-NM interface, which could be a driving force of the spin current, namely, thermal spin injection [17,18]. Since we have demonstrated that CoFe-based ferromagnetic alloys show high thermal-spin-injection efficiency because of its large spin-dependent Seebeck coefficient with a favorable band structure [19], we may develop a highly efficient spin-injection technique by combining FMR heating with the appropriate material. In this paper, we evaluate the performance of dynamical thermal spin injection based on FMR heating.

II. EXPERIMENTAL PROCEDURES

In this study, we adapt a $Co_{40}Fe_{40}B_{20}$ film as the FMR-heating layer because the large electrical resistivity for the (Co,Fe)B film with a relatively small anisotropic magnetoresistance effect suppresses the spurious signals for the spin-current transport [20]. First, we evaluate the temperature increase due to the FMR of the (Co,Fe)B. We prepare a (Co,Fe)B strip underneath a Cu waveguide on a glass substrate. Here, the (Co,Fe)B strip, whose width, length, and thickness are 7.5 μm, 500 μm, and 30 nm, respectively, is prepared by using an ultra-high-vacuum magnetron-sputtering system under a base pressure of 10^{-6} Pa. The electrical resistivity for (Co,Fe)B is 110 $\mu\Omega$ cm, indicating an amorphous structure. The Cu waveguide, 8.5 μm wide, 500 μm long, and 100 nm thick, is deposited by Joule evaporation. Figure 1(a) shows schematic illustrations of the device structure for the temperature evaluation. We emphasize that the electrical resistivity for Cu is approximately 2.3 $\mu\Omega$ cm at room temperature, which is approximately 50 times smaller than that for (Co,Fe)B. This means that the current flowing in the (Co,Fe)B layer of the bilayer system is negligibly small because of the large difference between the electrical resistivity and the film thickness.

III. RESULTS AND DISCUSSIONS

A. Evaluation of the FMR-heating effect

We measure the resistance of a Cu waveguide on a (Co,Fe)B strip under microwave irradiation as a function of the static magnetic field along the (Co,Fe)B strip by using a standard lock-in technique. Figure 1(b) shows a representative result of the field dependence of a resistance under a 12-GHz microwave irradiation with a power of 100 mW. We can see clear peak signatures around the FMR fields, depending on the microwave frequency, thus confirming the presence of the FMR-heating effect of the (Co,Fe)B

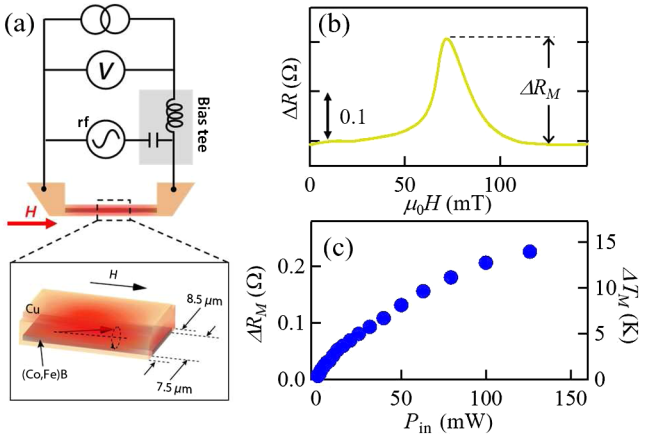

FIG. 1. FMR-heating effect. (a) Circuit diagram for the resistance measurement under rf current injection together with a schematic illustration of the FMR-heating effect. (b) Representative resistance spectrum due to the FMR-heating effect. (c) Maximum resistance change ΔR_M and the temperature change ΔT_M due to FMR heating as a function of the input power P with a frequency of 11 GHz.

strip. From the analysis of the resistance spectra with the temperature dependence of the Cu resistance, we are quantitatively able to estimate the temperature change during the FMR [16]. Here, we define ΔR_M as the maximum value of the resistance change due to the FMR. Here, we can convert ΔR_M to the temperature change ΔT_M by using the equation $\Delta T_M \approx 885 \Delta R_M / R_{RT}$, with the room-temperature resistance R_{RT}. Figure 1(c) shows ΔR_M as a function of the input rf power. Although the linewidth of the resistance spectra for (Co,Fe)B is much smaller than that for $Co_{43}Fe_{54}Al_3$, the ΔT_M value for (Co,Fe)B is larger than that of (Co,Fe)Al [16]. This is the case because the precession amplitude (the cone angle or dynamic susceptibility) increases with a decreasing damping constant, as described later [21,22]. Thus, the ferromagnet with the lower damping constant is suitable for inducing efficient FMR heating with high-frequency selectivity, while the larger damping constant contributes to the broad linewidth of the resistance peak.

B. Dynamical thermal spin injection due to FMR heating

We then experimentally investigate the dynamical thermal spin injection due to the FMR heating in a (Co, Fe)B/Pt bilayer system. As schematically shown in Fig. 2(a), the Cu waveguide, which is a microwave generator for the FMR, is prepared on the (Co, Fe)B/Pt bilayer film. Since the temperature of the ferromagnetic metal (Co,Fe)B increases under the FMR condition, the heat flow perpendicular to the interface between the (Co,Fe)B and Pt bilayers is generated. This action results in the thermal spin injection from the (Co,Fe)B layer into the Pt one. The spin current injected from the (Co,Fe)B layer into the Pt layer is converted to the electrical charge

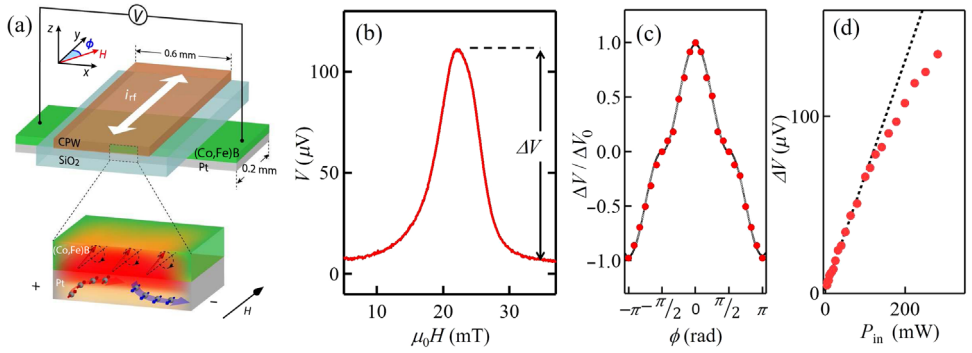

FIG. 2. Dynamical thermal spin injection. (a) Schematic illustration of a spin Hall device operated by dynamical thermal spin injection due to FMR heating. (b) Representative result of the field dependence of the electric voltage induced by the inverse spin Hall voltage under microwave irradiation. (c) Angular dependence of the normalized signal change due to the inverse spin Hall signal. (d) Power dependence of the output voltage due to the inverse spin Hall effect. The dotted line represents a linear variation of the output voltage.

current via the inverse spin Hall effect (SHE) of the Pt layer [4,23]. The (Co, Fe)B/Pt bilayer film is prepared on a FZ-Si substrate by using an ultra-high-vacuum magnetron-sputtering system. The lateral dimension of the bilayer film patterned by the stencil mask is 200 μm wide and 600 μm long. The thicknesses of the (Co,Fe)B and Pt layers are 40 and 10 nm, respectively. The waveguide and the bilayer are electrically separated by inserting a 100-nm-thick SiO_2 film. Here, the resistance of the bilayer film is as low as 33 Ω.

When the spin direction of the injected spin current is aligned with the x axis, the injected spin current flowing along z axis is converted to the electrical charge current along the Pt wire (x axis) through the inverse spin Hall effect, as is schematically shown in Fig. 2(a). With an open-circuit condition, we can detect spin current as the electrical voltage along the Pt wire. Figure 2(b) shows the field dependence of the electrical voltage along the Pt wire under the microwave irradiation of 6 GHz. A clear voltage peak is observed at $\mu_0 H = 20$ mT, which is exactly same as the FMR field under 6-GHz microwave irradiation.

To obtain more definite evidence, the angular dependence of the overall signal change is investigated by changing the direction of the static magnetic field. Here, we define the angle ϕ, which is the difference between the direction of the ac current and the static magnetic field. The angular dependence of the inverse spin Hall effect is known to show cosine dependence because the direction of the induced charge current is given by the vector product $\boldsymbol{s} \times \boldsymbol{I}_s$, where $\boldsymbol{s}$ and $\boldsymbol{I}_s$ are the electron spin and the spin current, respectively [4,6,23], We note that, in the present device configuration, the direction of the ac magnetic field is fixed along the x axis. Therefore, when the direction of the static magnetic field is rotated by an angle ϕ, the effective magnitude of the ac magnetic field should show $\cos\phi$ dependence. In such a situation, the output voltage due to the spin Hall effect is proportional to $|\cos\phi|\cos\phi$. As can be seen in Fig. 2(c), the angular dependence of the normalized signal change is well reproduced by $|\cos\phi|\cos\phi$, strongly supporting the spin Hall nature of the voltage. However, the observed characteristics can also be understood by the dynamical spin injection based on the spin pumping. Therefore, we have to find out the specific signature of the thermal spin injection in order to identify the proper mechanism of the dynamical spin injection in a FM/NM bilayer system.

Figure 2(d) shows the maximum voltage change ΔV vs the input power $P_{\rm in}$. ΔV increases linearly below the input power of 200 mW, but it starts to deviate above the input power of 200 mW. This kind of saturation tendency was not observed in previous reports on spin-pumping experiments because the efficiency of the spin pumping increases an increasing precession angle. On the other hand, in the thermal-spin-injection case, since the spin-injection efficiency is proportional to the longitudinal component of the magnetization, increasing the precessional cone angle contributes to reducing the spin-injection efficiency. Since we can see a similar power dependence in the FMR-heating effect shown in Fig. 1(d), this unique signature suggests that FMR heating is the main contribution to the output voltage. Here, the threshold power is much larger than that for the FMR-heating device. This is the case because the excitation efficiency for the spin Hall device is much smaller than that of the FMR-heating device. It also should be noted that the voltage change due to the inverse spin Hall effect exceeds 100 μV, which is relatively large compared to the values obtained in the similar metallic bilayer system based on the spin pumping. This result implies that the thermal spin injection is more efficient than the spin pumping in a material with a large spin-dependent Seebeck effect.

As mentioned before, the bilayer sample structure used in our study is the same as that for the spin-pumping experiments [4,23–26]. Therefore, both the thermal spin injection and the spin pumping are possible mechanisms for generating the spin current in this structure. To distinguish the dominant mechanism of the spin-current generation in the present experiment, we analyze the

experimental data more quantitatively and perform additional experiments. First, to properly evaluate the performance of the present spin Hall device, we introduce the normalized spin Hall voltage η, which is given by the overall change of the spin Hall voltage under the open-circuit condition divided by the series resistance of the bilayer system for a unit width Rw, namely, $V/(Rw)$. This is the case because the output spin Hall voltage depends on the geometry and the device dimension. According to the simple spin-diffusion model, the output spin Hall voltage V is given by $\lambda\alpha_{\mathrm{SHE}}i_{S0}Rw$. Here, R is the resistance along the z axis for the Pt layer underneath the waveguide, λ is the spin-diffusion length for the Pt layer, α_{SHE} is the spin Hall angle for the Pt layer, and i_{S0} is the injected spin current density at the interface. Therefore, we obtain $\eta = \lambda\alpha_{\mathrm{SHE}}i_{S0}$, which is determined by the material parameter without any geometrical parameters. Consequently, we can fairly compare the spin-injection efficiency by using the normalized spin Hall voltage η.

Figure 3(c) shows the representative curve of the field dependence of the normalized spin Hall voltage η under a microwave irradiation of 6 GHz with an input power 100 mW. We note that the input power is 100 times larger than the absorption power, which is the effective excitation power for the FMR, as we address later. The obtained amplitude of the signal is as high as 23 $\mathrm{mV\,\Omega^{-1}\,m^{-1}}$. This value is relatively high compared to Py/NM bilayer systems (0.3–5 $\mathrm{mV\,\Omega^{-1}\,m^{-1}}$ for Py/Pt bilayers, approximately 1 $\mathrm{mV\,\Omega^{-1}\,m^{-1}}$ for Py/Ta bilayers and about 7 $\mathrm{mV\,\Omega^{-1}\,m^{-1}}$ for Py/Pd bilayers [24–27]) and 0.1–1 $\mathrm{mV\,\Omega^{-1}\,m^{-1}}$ for yttrium iron garnet/NM bilayer systems [28–30], where the spin pumping can be considered the main mechanism.

To obtain a more clear signature for the thermal spin injection, we also investigate the inverse spin Hall effect under the dynamical spin injection in a Pt/(Co, Fe)B bilayer system, where the (Co,Fe)B layer and the Pt film are deposited on the substrate with a configuration opposite to that in the previous experiment. From the vector-network-analyzer measurements, as can be seen in Figs. 3(a) and 3(b), we confirm that the resonant frequency and the frequency linewidth are not significantly different between the two samples. In the Pt/(Co, Fe)B/Si substrate system, since a partial heat flow from the (Co,Fe)B layer diffuses into the substrate directly without passing through the Pt film in this configuration, the magnitude of the thermally excited spin current injected into the Pt film should decrease, resulting in the reduction of the inverse spin Hall voltage from the previous experiment. On the other hand, if the main mechanism for the spin injection is spin pumping, the spin Hall voltage should not change, because of negligibly small spin pumping into the Si substrate.

Figure 3(d) shows the normalized inverse spin Hall voltage in the Pt/(Co, Fe)B system. The sign of the voltage is also reversed from the previous experiment because the flowing direction of the spin current is the opposite of the previous experiment using a (Co, Fe)B/Pt/Si substrate system. Moreover, we can clearly confirm the significant reduction of the induced voltage. By separating the symmetric and antisymmetric contributions, we can obtain a more clear signature of the thermal spin injection. As can be seen in Figs. 3(e) and 3(f), the symmetric signal shows a significant reduction, although the antisymmetric signal does not change so much. This is the case because the heat flow from the (Co,Fe)B layer into the Pt wire is reduced. These stacking-order dependences cannot be understood by the spin-pumping model. The observed tendency is the opposite of the previous study on stacking-order dependences [23], where the eddy current produces an additional rf magnetic field. This fact may be due to the thinner thickness of the Pt film and the smaller overlap area between the waveguide and the (Co, Fe)B/Pt bilayer.

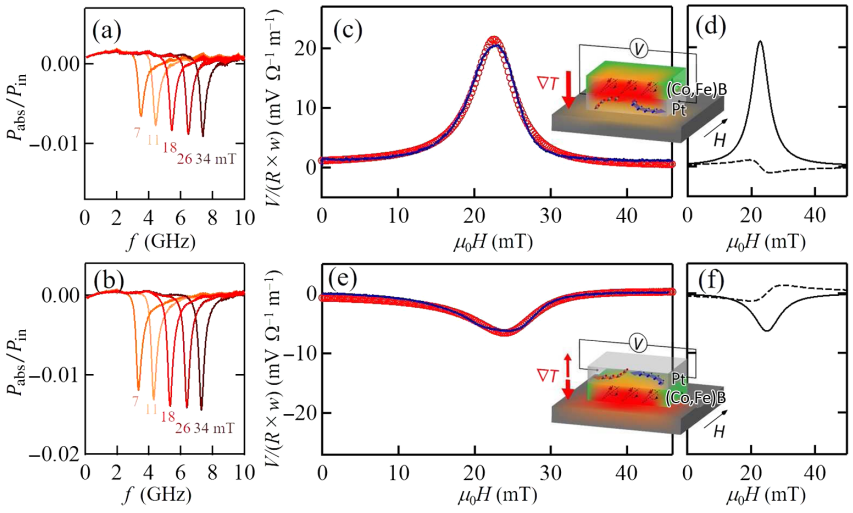

FIG. 3. Distinguishing between thermal spin injection and spin pumping. FMR spectra under various magnetic fields in (a) the (Co, Fe)B/Pt/Si substrate sample and (b) the Pt/(Co, Fe)B/Si substrate sample. (c) Field dependence of the normalized spin Hall signal induced in (Co, Fe)B/Pt/Si substrate sample under microwave irradiation. The vertical axis is the voltage normalized by the resistance and the width of the bilayer. (d) Field dependence of the normalized spin Hall signal induced in Pt/(Co, Fe)B/Si substrate sample under microwave irradiation. (e) Separation of symmetric and antisymmetric contributions to the induced electric voltage in the (Co, Fe)B/Pt/Si substrate sample. (f) Separation of symmetric and antisymmetric contributions to the induced electric voltage in the Pt/(Co, Fe)B/Si substrate sample.

It also should be noted that these results exclude the possibility of the anomalous Nernst effect (ANE) from the (Co,Fe)B layer because the ANE should not show stacking-order dependence. Although the spin pumping also contributes to the generation of the spin current, these results strongly suggest that the dominant contribution of the dynamical spin injection in our (Co, Fe)B/Pt system is the thermally excited spin current associated with the large spin-dependent Seebeck effect. We would emphasize that the non-negligible contribution from thermal spin injection should be considered even in a NiFe/Pt bilayer system, which is widely utilized in spin-pumping experiments [24–26]. The estimated spin Hall angle based on a spin-pumping mechanism may be overestimated because the thermally excited spin current is neglected.

IV. CONCLUSION

In this work, we show that the FMR-heating effect is effectively excited by the microwave irradiation under the bias magnetic field in a (Co,Fe)B film. We demonstrate that the inverse spin Hall effect is induced by the thermal spin injection driven by the FMR-heating effect in a (Co, Fe)B/Pt bilayer system. The obtained voltage due to the inverse spin Hall effect is relatively large compared to a similar bilayer system based on spin pumping, indicating the efficient thermal spin injection from (Co,Fe)B. The stacking-order dependences strongly support the fact that the spin current is generated by thermal spin injection due to the FMR heating of the (Co,Fe)B film.

ACKNOWLEDGMENTS

This work is partially supported by Grant-in-Aid for Scientific Research on Innovative Area, "Nano Spin Conversion Science" (JP26103002) and that for Scientific Research (S) (JP25220605), and Canon Foundation.

[1] S. A. Wolf, D. D. Awschalom, R. A. Buhrman, J. M. Daughton, S. von Molnár, M. L. Roukes, A. Y. Chtchelkanova, and D. M. Treger, Spintronics: A spin-based electronics vision for the future, Science **294**, 1488 (2001).

[2] *Handbook of Spin Transport and Magnetism*, edited by E. Y. Tsymbal and I. Žutić (CRC Press, Boca Raton, 2011).

[3] J. E. Hirsch, Spin Hall Effect, Phys. Rev. Lett. **83**, 1834 (1999).

[4] E. Saitoh, M. Ueda, H. Miyajima, and G. Tatara, Conversion of spin current into charge current at room temperature: Inverse spin-Hall effect, Appl. Phys. Lett. **88**, 182509 (2006).

[5] S. O. Valenzuela and M. Tinkham, Direct electronic measurement of the spin Hall effect, Nature (London) **442**, 176 (2006).

[6] T. Kimura, Y. Otani, T. Sato, S. Takahashi, and S. Maekawa, Room-Temperature Reversible Spin Hall Effect, Phys. Rev. Lett. **98**, 156601 (2007).

[7] T. Kimura, Y. Otani, and J. Hamrle, Switching Magnetization of a Nanoscale Ferromagnetic Particle Using Nonlocal Spin Injection, Phys. Rev. Lett. **96**, 037201 (2006).

[8] A. Hoffmann, Pure spin-currents, Phys. Status Solidi C **4**, 4236 (2007).

[9] S. Mizukami, Y. Ando, and T, Miyazaki, effect of spin diffusion on gilbert damping for a very thin permalloy layer in Cu/Permalloy/Cu/Pt films, Phys. Rev. B **66**, 104413 (2002).

[10] Y. Tserkovnyak, A, Brataas, and G. E. W. Bauer, Enhanced Gilbert Damping in Thin Ferromagnetic Films, Phys. Rev. Lett. **88**, 117601 (2002).

[11] X. Liu, W. Zhang, J. M. Carter, and G. Xiao, Ferromagnetic resonance and damping properties of CoFeB thin films as free layers in MgO-based magnetic tunnel junctions, J. Appl. Phys. **110**, 033910 (2011).

[12] B. Kuanr, R. E. Camley, and Z. Celinski, Narrowing of the frequency-linewidth in structured magnetic strips: Experiment and theory, Appl. Phys. Lett. **87**, 012502 (2005).

[13] W. Zhang, W. Han, X. Jiang, S. Yang, and S. S. P. Parkin, Role of transparency of platinum-ferromagnet interfaces in determining the intrinsic magnitude of the spin Hall effect, Nat. Phys. **11**, 496 (2015).

[14] M. Jamali, A. K. Smith, and J. Wang, Nonreciprocal behavior of the spin pumping in ultra-thin film of CoFeB, J. Appl. Phys. **119**, 133903 (2016).

[15] D. Wei, M. Obstbaum, M. Ribow, C. H. Back, and G. Woltersdorf, Spin Hall voltages from a.c. and d.c. spin currents, Nat. Commun. **5**, 3768 (2014).

[16] K. Yamanoi, Y. Yokotani, and T. Kimura, Heat dissipation due to ferromagnetic resonance in a ferromagnetic metal monitored by electrical resistance measurement, Appl. Phys. Lett. **107**, 182410 (2015).

[17] A. Slachter, F. L. Bakker, J. Adam, and B. J. van Wees, Thermally driven spin injection from a ferromagnet into a non-magnetic metal, Nat. Phys. **6**, 879 (2010).

[18] G. Choi, B. Min, K. Lee, and D. G. Cahill, Spin current generated by thermally driven ultrafast demagnetization, Nat. Commun. **5**, 4334 (2014).

[19] S. Hu, H. Itoh, and T. Kimura, Efficient thermal spin injection using CoFeAl nanowire, NPG Asia Mater. **6**, e127 (2014).

[20] S. U. Jen, Y. D. Yao, Y. T. Chen, J. M. Wu, C. C. Lee, T. L. Tsai, and Y. C. Chang, Magnetic and electrical properties of amorphous CoFeB films, J. Appl. Phys. **99**, 053701 (2006).

[21] G. Counil, J. Kim, T. Devolder, C. Chappert, K. Shigeto, and Y. Otani, Spin wave contributions to the high-frequency magnetic response of thin films obtained with inductive methods, J. Appl. Phys. **95**, 5646 (2004).

[22] A. Azevedo, R. O. Cunha, F. Estrada, O. Alves Santos, J. B. S. Mendes, L. H. Vilela-Leão, R. L. Rodríguez-Suárez, and S. M. Rezende, Electrical detection of ferromagnetic resonance in single layers of permalloy: Evidence of magnonic charge pumping, Phys. Rev. B **92**, 024402 (2015).

[23] V. Vlaminck, J. E. Pearson, S. D. Bader, and A. Hoffmann, Detection and quantification of inverse spin Hall effect from spin pumping in permalloy/normal metal bilayers, Phys. Rev. B **88**, 064414 (2013).

[24] K. Ando, S. Takahashi, J. Ieda, Y. Kajiwarea, H. Nakayama, T. Yoshino, K. Harii, Y. Fujikawa, S. Maekawa, and E. Saitoh, Inverse spin-Hall effect induced by spin pumping in metallic system, J. Appl. Phys. **109**, 103913 (2011).

[25] O. Mosendz, V. Vlaminck, J. E. Pearson, F. Y. Fradin, G. E. W. Bauer, S. D. Bader, and A. Hoffmann, Detection and quantification of inverse spin Hall effect from spin pumping in permalloy/normal metal bilayers, Phys. Rev. B **82**, 214403 (2010).

[26] P. Deorani and H. Yang, Role of spin mixing conductance in spin pumping: Enhancement of spin pumping efficiency in Ta/Cu/Py structures, Appl. Phys. Lett. **103**, 232408 (2013).

[27] O. Mosendz, J. E. Pearson, F. Y. Fradin, G. E. W. Bauer, S. D. Bader, and A. Hoffmann, Quantifying Spin Hall Angles from Spin Pumping: Experiments and Theory, Phys. Rev. Lett. **104**, 046601 (2010).

[28] V. Castel, N. Vlietstra, Ben. J. Youssef, and B. J. van Wees, Platinum thickness dependence of the inverse spin-Hall voltage from spin pumping in a hybrid yttrium iron garnet/platinum system, Appl. Phys. Lett. **101**, 132414 (2012).

[29] C. Hahn, G. de Loubens, O. Klein, M. Viret, V. V. Naletov, and J. Ben Youssef, Comparative measurements of inverse spin Hall effects and magnetoresistance in YIG/Pt and YIG/Ta, Phys. Rev. B **87**, 174417 (2013).

[30] H. L. Wang, C. H. Du, Y. Pu, R. Adur, P. C. Hammel, and F. Y. Yang, Scaling of Spin Hall Angle in 3*d*, 4*d*, and 5*d* Metals from $Y_3Fe_5O_{12}$/Metal Spin Pumping, Phys. Rev. Lett. **112**, 197201 (2014).